

Original Article  
Gastroenterology &  
Hepatology



# Radiomics Analysis of Magnetic Resonance Proton Density Fat Fraction for the Diagnosis of Hepatic Steatosis in Patients With Suspected Non-Alcoholic Fatty Liver Disease

Ki Choon Sim ,<sup>1</sup> Min Ju Kim ,<sup>1</sup> Yongwon Cho ,<sup>1,2</sup> Hyun Jin Kim ,<sup>1</sup> Beom Jin Park ,<sup>1</sup> Deuk Jae Sung ,<sup>1</sup> Na Yeon Han ,<sup>1</sup> Yeo Eun Han ,<sup>1</sup> Tae Hyung Kim ,<sup>3</sup> and Yoo Jin Lee ,<sup>4</sup>

<sup>1</sup>Department of Radiology, Korea University Anam Hospital, Korea University College of Medicine, Seoul, Korea

<sup>2</sup>AI Center, Korea University Anam Hospital, Korea University College of Medicine, Seoul, Korea

<sup>3</sup>Department of Gastroenterology, Korea University Ansan Hospital, Korea University College of Medicine, Ansan, Korea

<sup>4</sup>Department of Pathology, Korea University Anam Hospital, Korea University College of Medicine, Seoul, Korea

OPEN ACCESS

Received: Aug 2, 2022

Accepted: Sep 23, 2022

Published online: Nov 16, 2022

\*Address for Correspondence:

Min Ju Kim, MD, PhD

Department of Radiology, Korea University Anam Hospital, Korea University College of Medicine, 73 Goryeodae-ro, Seongbuk-gu, Seoul 02841, Korea.

Email: dr.minjukim@gmail.com

© 2022 The Korean Academy of Medical Sciences.

This is an Open Access article distributed under the terms of the Creative Commons Attribution Non-Commercial License (<https://creativecommons.org/licenses/by-nc/4.0/>) which permits unrestricted non-commercial use, distribution, and reproduction in any medium, provided the original work is properly cited.

ORCID iDs

Ki Choon Sim

<https://orcid.org/0000-0002-3344-8018>

Min Ju Kim

<https://orcid.org/0000-0003-0979-9835>

Yongwon Cho

<https://orcid.org/0000-0001-8092-5799>

Hyun Jin Kim

<https://orcid.org/0000-0002-2078-5058>

## ABSTRACT

**Background:** This study aimed to assess the diagnostic feasibility of radiomics analysis based on magnetic resonance (MR)-proton density fat fraction (PDFF) for grading hepatic steatosis in patients with suspected non-alcoholic fatty liver disease (NAFLD).

**Methods:** This retrospective study included 106 patients with suspected NAFLD who underwent a hepatic parenchymal biopsy. MR-PDFF and MR spectroscopy were performed on all patients using a 3.0-T scanner. Following whole-volume segmentation of the MR-PDFF images, 833 radiomic features were analyzed using a commercial program. Radiologic features were analyzed, including median and mean values of the multiple regions of interest and variable clinical features. A random forest regressor was used to extract the important radiomic, radiologic, and clinical features. The model was trained using 20 repeated 10-fold cross-validations to classify the NAFLD steatosis grade. The area under the receiver operating characteristic curve (AUROC) was evaluated using a classifier to diagnose steatosis grades.

**Results:** The levels of pathological hepatic steatosis were classified as low-grade steatosis (grade, 0–1; n = 82) and high-grade steatosis (grade, 2–3; n = 24). Fifteen important features were extracted from the radiomic analysis, with the three most important being wavelet-LLL neighboring gray tone difference matrix coarseness, original first-order mean, and 90th percentile. The MR spectroscopy mean value was extracted as a more important feature than the MR-PDFF mean or median in radiologic measures. Alanine aminotransferase has been identified as the most important clinical feature. The AUROC of the classifier using radiomics was comparable to that of radiologic measures ( $0.94 \pm 0.09$  and  $0.96 \pm 0.08$ , respectively).

**Conclusion:** MR-PDFF-derived radiomics may provide a comparable alternative for grading hepatic steatosis in patients with suspected NAFLD.

**Keywords:** Radiomics; Liver Steatosis; Magnetic Resonance Imaging; Proton Density Fat Fraction; Non-alcoholic Fatty Liver Disease

Beom Jin Park <https://orcid.org/0000-0002-7289-3683>Deuk Jae Sung <https://orcid.org/0000-0002-5025-3052>Na Yeon Han <https://orcid.org/0000-0001-8537-8165>Yeo Eun Han <https://orcid.org/0000-0002-3922-9326>Tae Hyung Kim <https://orcid.org/0000-0002-7747-4293>Yoo Jin Lee <https://orcid.org/0000-0003-3830-7051>**Disclosure**

The authors have no potential conflicts of interest to disclose.

**Author Contributions**

Conceptualization: Kim MJ. Data curation: Sim KC, Kim MJ, Kim HJ. Formal analysis: Sim KC, Kim TH, Lee YJ. Methodology: Sim KC, Kim MJ, Cho Y. Supervision: Kim MJ. Validation: Park BJ, Sung DJ, Han NY, Han YE. Writing - original draft: Sim KC, Kim HJ. Writing - review & editing: Sim KC, Kim MJ, Cho Y.

**INTRODUCTION**

Steatosis is a common manifestation of various liver diseases. Among them, non-alcoholic fatty liver disease (NAFLD) is an emerging public health issue, and it has been reported in approximately 25% of the general population. NAFLD has a wide spectrum, ranging from asymptomatic to inflammation with or without fibrosis.<sup>1-4</sup> Recent studies have reported that superimposed liver steatosis is associated with a higher risk of liver cirrhosis or hepatocellular carcinoma.<sup>5,6</sup> Therefore, detection and quantification of liver steatosis in patients with suspected NAFLD is important to determine prognosis and guide treatment decisions.

A percutaneous liver parenchymal biopsy is the gold standard method for staging steatosis and fibrosis; however, it has several disadvantages, including invasiveness, risk of bleeding, and risk of sampling error due to the heterogeneity of the disease distribution.<sup>7-9</sup> Various non-invasive quantitative methods, including ultrasound and magnetic resonance imaging (MRI), have been developed and used to address the limitations of liver parenchymal biopsies. In particular, the magnetic resonance (MR)-proton density fat fraction (PDFF) is considered a non-invasive reference standard for assessing liver fat content.<sup>4,10-12</sup> However, conventional post-processing MR-PDFF methods are limited by the use of mean signal intensity values by drawing the region of interest (ROI).<sup>13,14</sup>

Radiomics enables the analysis of images beyond visual inspection by extracting dozens to hundreds of quantitative features.<sup>15</sup> The application of radiomics in liver disease has focused on the prediction and differentiation of various tumors or fibrosis assessment<sup>16,17</sup>; however, radiomic analysis of hepatic steatosis using MR-PDFF in patients with NAFLD has not yet been conducted. Therefore, we hypothesized that radiomic features extracted from MR-PDFF images would allow a more accurate assessment of hepatic steatosis than conventional ROI methods or the use of clinical data. Consequently, we investigated the diagnostic performance of several modalities including MR-PDFF radiomics for detection of hepatic steatosis grade  $\geq 2$  in patients with suspected NAFLD.

**METHODS****Study participants**

Patients with suspected NAFLD in our institution's gastroenterology department who underwent MR-PDFF between November 2017 and May 2020 were included in the study. The inclusion criteria were as follows: 1) age  $\geq 18$  years; 2) suspected hepatic steatosis on ultrasound imaging; and 3)  $\leq 60$  days between MR-PDFF and liver biopsy. The exclusion criteria were as follows: 1) history of alcohol consumption;  $\geq 30$  g/day for man and  $\geq 20$  g/day for woman; 2) history of chronic liver diseases such as chronic viral hepatitis B or C infection, autoimmune hepatitis, and primary sclerosing cholangitis; 3) history of major liver surgery such as liver transplantation and hemihepatectomy; or 4) unavailability of liver biopsy. **Fig. 1** shows a flow diagram of the study population and **Table 1** shows their demographic and clinical characteristics.

The clinical features collected from the patients, including age, sex, weight, height, and blood test results (alanine aminotransferase [ALT], aspartate aminotransferase [AST], triglyceride, low-density lipoprotein, and platelet count) obtained within 1 month of MR-PDFF were evaluated. Body mass index and aspartate aminotransferase-to-platelet ratio index were also calculated.

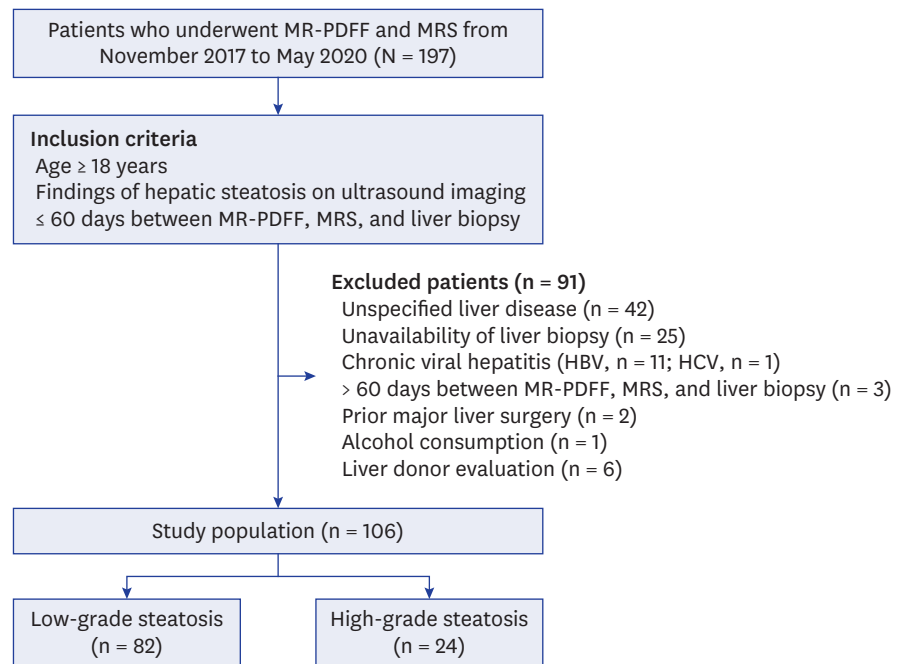


**Fig. 1.** Flow diagram for the study population. MR-PDFF = magnetic resonance-proton density fat fraction, MRS = magnetic resonance spectroscopy, HBV = hepatitis B virus, HCV = hepatitis C virus.

**Table 1.** Demographic characteristics of patients with suspected non-alcoholic fatty liver disease

Characteristics	Low-grade steatosis (n = 82)	High-grade steatosis (n = 24)	P value
Sex (men:women)	53:29	18:6	0.342
Hypertension (+tive)	27	5	0.256
Diabetes mellitus (+tive)	18	3	0.307
Age, yr	47.4 ± 13.2	35.4 ± 11.7	< 0.001
BMI, kg/m <sup>2</sup>	27.4 ± 4.2	30.8 ± 6.5	0.004
AST, IU/L	46.5 ± 32.4	64.9 ± 32.3	0.016
ALT, IU/L	69.2 ± 57.6	128.9 ± 73.1	< 0.001
AST/ALT ratio	0.84 ± 0.55	0.57 ± 0.16	0.022
GGT, IU/L	60.2 ± 54.6	67.7 ± 58.2	0.562
ALP, IU/L	82.6 ± 24.7	78.6 ± 20.9	0.473
Total bilirubin, mg/dL	0.7 ± 0.3	0.8 ± 0.5	0.217
Albumin, g/dL	4.2 ± 0.4	4.5 ± 0.4	0.004
Ferritin, ng/mL	187.2 ± 167.9	304.1 ± 240.5	0.014
Total TG, mg/dL	176.4 ± 136.6	222.2 ± 117.3	0.149
LDL, mg/dL	115.4 ± 30.6	136.3 ± 29.5	0.020
HDL, mg/dL	42.0 ± 8.7	41.1 ± 6.6	0.649
Platelet count, × 10 <sup>9</sup> /L	235.2 ± 61.3	258.3 ± 70.4	0.085
APRI	0.56 ± 0.47	0.67 ± 0.38	0.303
NAS	2.5 ± 1.4	4.5 ± 1.1	< 0.001

BMI = body mass index, AST = aspartate aminotransferase, ALT = alanine aminotransferase, GGT = gamma-glutamyl transferase, ALP = alkaline phosphatase, TG = triglyceride, LDL = low-density lipoprotein, HDL = high-density lipoprotein, APRI = aspartate aminotransferase to platelet ratio index, NAS = non-alcoholic fatty liver disease activity score.

### The histopathological grade of hepatic steatosis

Histopathological examination of the liver serves as the gold standard for liver steatosis. One hundred and four patients underwent a percutaneous liver biopsy using an 18-gauge semi-automated biopsy needle with a penetration depth of 20 mm targeting segment 5/6, and two biopsy cores were obtained. The remaining two patients underwent a surgical biopsy during

cholecystectomy and donor hemihepatectomy. Histological preparations of liver biopsies were retrospectively reviewed by one pathologist (7 years of experience) blinded to the clinical data and MR-PDFF results. NAFLD activity score was graded according to the criteria of Kleiner et al.<sup>8</sup> Liver steatosis was graded according to the percentage of fat within the hepatocytes: grade 0 (healthy, < 5%), grade 1 (mild, 5–33%), grade 2 (moderate, 34–66%), and grade 3 (severe, > 66%).<sup>14</sup> The stage of pathological hepatic steatosis was classified as low-grade (grade 0 or grade 1) or high-grade steatosis (grade 2 or grade 3).<sup>18–20</sup>

### MRI acquisition

All MRI scans were performed using a 3.0-T system (Magnetom Skyra; Siemens Healthineers, Erlangen, Germany) with a 30-channel body coil. MR-PDFF was performed according to a previously described protocol<sup>21–23</sup> using commercial hardware and software (Resoundant Inc., Rochester, MN, USA; Syngo MR E11, Siemens Healthineers).<sup>13</sup> For PDFF, complex-based chemical shift-encoded water-fat reconstruction techniques were used with six-echo three-dimensional gradient-recalled-echo images, an imaging matrix of 160 × 115, field of view of 380 × 304, and slice thickness of 3 mm without gaps. A low flip angle (4°) was used to minimize the T1 bias between fat and water.<sup>12,23</sup> A sufficient scan range was used to include all livers. PDFF maps were automatically reconstructed using the vendor's algorithm with the T2\* correction calculated from signal decay and a multipeak fat model.<sup>24</sup>

Furthermore, the MRS of the liver included in the vendor's algorithm was performed in the right hepatic lobe randomly by a radiologic technologist from three rectangular ROIs for reference to the MR-PDFF value.

### MR image segmentation and analysis processing

Before starting the segmentation process, three radiologists were trained using a software applicator to improve the segmentation accuracy. In addition, all radiologists preliminarily discussed about 15 cases and decided on consensus and optimization of segmentation. Three radiologists were randomly assigned to perform whole-volume segmentation. Segmentation was performed as carefully as possible to exclude the major hepatic and portal veins, hepatic fissures, and gallbladder (Fig. 2). As a result, whole-volume segmentation of fat fraction images of MR-PDFF was completed by three radiologists (two abdominal radiologists with 22 years [n = 21] and 10 years [n = 28] of clinical experience, respectively, and second year resident in radiology [n = 57]) using a commercial program, AVIEW (version 1.0.32.12; Coreline Soft, Seoul, Korea).

Eight or nine circular ROIs were evaluated using the fat fraction image of MR-PDFF, which has been shown to correlate accurately with liver histology and MRS.<sup>21,25–27</sup> ROI areas were maintained at approximately 300–350 mm<sup>2</sup> and manually drawn while avoiding the edges of the liver and major vessels (Fig. 3).<sup>28</sup> All post-processing was performed using a commercial workstation by a gastrointestinal radiologist with 10 years of experience, who was blinded to the clinicopathological data. The liver steatosis values obtained from MR-PDFF were organized using the mean and median values, and the steatosis values were used as radiologic features.

For the three MRS values obtained during the MRI examination (Fig. 3), the mean value was also used as a radiologic feature.

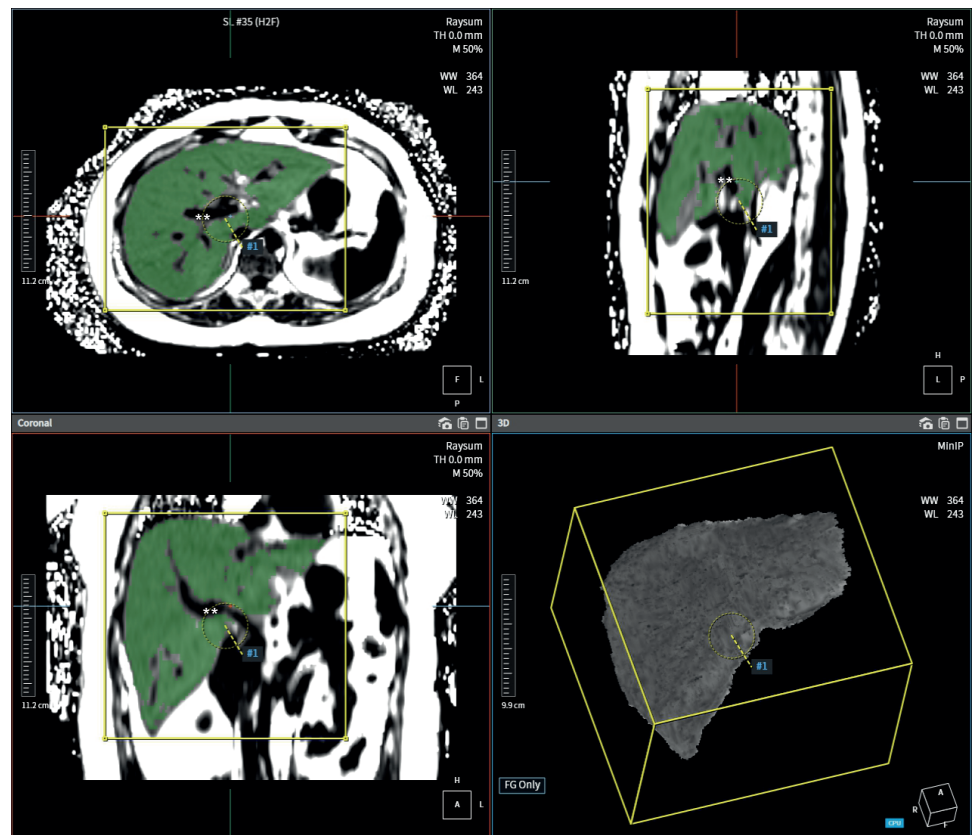


**Fig. 2.** A 30-year-old woman with non-alcoholic fatty liver disease. The work screen shows the completion of the whole-volume segmentation of the fat fracture image of the magnetic resonance-proton density fat fraction using a commercial program. Vascular structures such as portal veins (asterisk) are excluded and only the liver parenchyma indicated in green is accurately segmented.

### Radiomic feature extraction

Based on MR-PDFF data with whole-volume segmentation applied, several hundreds of radiomic features were analyzed using PyRadiomics 3.0.1 in Python (version 3.7.4; Python Software Foundation, Wilmington, DE, USA).<sup>29,30</sup> Fig. 4 illustrates the analysis pipeline. The features consisted of 14 shape features (two-dimensional and three-dimensional), 18 first-order features, and 73 texture features from the original image, as well as 144 first-order features ( $18 \times 8$ ) and 584 texture features ( $73 \times 8$ ) from eight types of wavelet-decomposition images, obtained with a high-pass filter (HLL, HLH, HHL, and HHH) and low-pass filter (LLL, LLH, LHL, and LHH). Wavelet-xyz indicates a combination of high-pass (H) and low-pass (L) filters, such as wavelet-low high low (LHL) or wavelet-high high low (HHL).<sup>31</sup> Therefore, a total of 833 radiomic features were extracted.

### Data analysis

#### Feature selection and classifier training

Radiomic, radiologic, and clinical features, which are important for grading hepatic steatosis in patients with suspected NAFLD, were selected using a random forest regressor in Python (version 3.6; Python Software Foundation) with the Scikit-learn package (<https://github.com/scikit-learn/scikit-learn>). Although many quantitative features can be extracted from radiomic, radiologic, and clinical data, they may be highly correlated or simply considered noise. Therefore, 20 repeated 10-fold stratified cross-validation and feature selection using a random

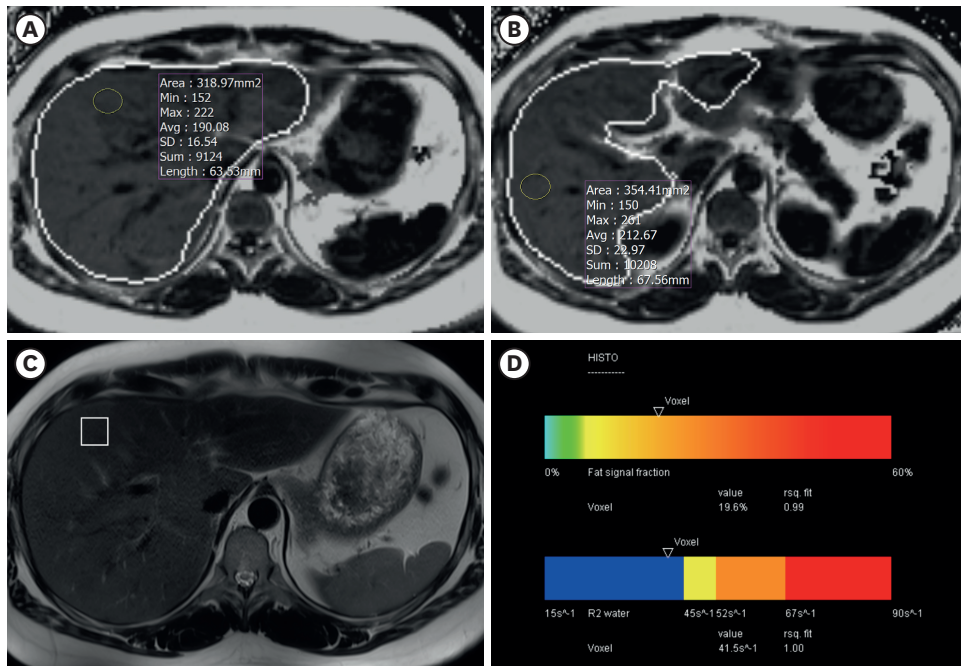


**Fig. 3.** A 33-year-old man with non-alcoholic fatty liver disease (hepatic steatosis grade 1 and 20% steatosis on histopathology). The liver steatosis values on the MR-PDFF are measured to be approximately 19.0% (A) and 21.3% (B). The value of liver steatosis on MRS is 19.6% (C, D). The MR-PDFF and MRS values measured at similar locations in segment 4a of the liver are almost identical (A, C). MR-PDFF = magnetic resonance-proton density fat fraction, MRS = magnetic resonance spectroscopy.

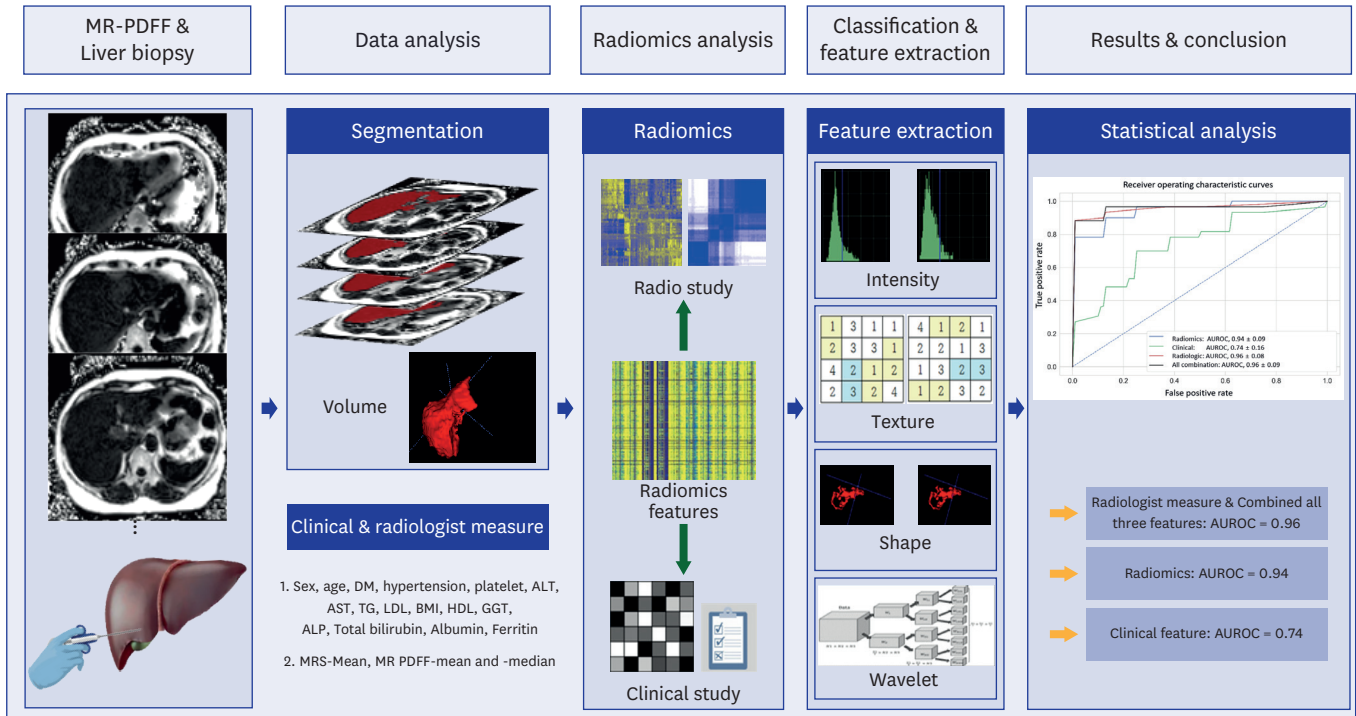


**Fig. 4.** Radiomics pipeline. MR-PDFF = magnetic resonance-proton density fat fraction, DM = diabetes mellitus, ALT = alanine aminotransferase, AST = aspartate aminotransferase, TG = triglyceride, LDL = low-density lipoprotein, BMI = body mass index, HDL = high-density lipoprotein, GGT = gamma-glutamyl transferase, ALP = alkaline phosphatase, MRS = magnetic resonance spectroscopy, AUROC = area under the receiver operating characteristic curve.

forest regressor were performed to avoid overfitting in the limited datasets.<sup>32</sup> A random forest classifier model<sup>33</sup> was trained to use these important features to classify steatosis grades as binary results. We evaluated the area under the receiver operating characteristic curve (AUROC) and classifier accuracy. The classifier diagnosed steatosis grade based on radiomic, radiologic, or clinical features or a combination of all features. Statistical differences in the AUROC according to each classifier were compared using a machine learning model with the Delong's test. Statistical significance was defined as a two-tailed  $P$  value  $< 0.05$ .

#### Statistical analyses

Demographic and clinical data of patients with suspected NAFLD were compared using the Mann-Whitney  $U$  test, paired  $t$ -test,  $\chi^2$  test, and Fisher's exact test. The intraclass correlation coefficient (ICC) verified the correlation between steatosis measurement methods. ICC values of 0.5–0.75, 0.75–0.9, and  $> 0.9$  were considered moderate, good, and excellent reliability, respectively.<sup>34</sup> The steatosis grade correlation between histology and MR-PDFF was evaluated using the weighted kappa test. Weighted-kappa value of  $< 0.20$ , 0.21–0.40, 0.41–0.60, 0.61–0.80, and 0.81–1.00 were considered poor, fair, moderate, good, and very good agreement. Statistical analyses were performed with SPSS Statistics 20.0 for Windows (IBM Corp., Armonk, NY, USA) or Medcalc 20.114 for Window (MedCalc Software Ltd., Ostend, Belgium). Statistical significance was defined as a two-tailed  $P$  value  $< 0.05$ .

#### Ethics statements

This retrospective study was approved by the Institutional Review Board of the Korea University Medical Center (approval number: 2020AN0387), and informed patient consent for research was waived. All research and data collection procedures adhered to the tenets of the Declaration of Helsinki.

## RESULTS

#### Patients' demographics

The demographic characteristics of patients with suspected NAFLD are presented in **Table 1**. As mentioned previously, 106 patients were enrolled in this study (**Fig. 1**). The mean interval between MR-PDFF and liver biopsies was 2.66 (range, 0–53) days. In 92 patients, the interval between MR-PDFF and liver biopsy was  $< 3$  days. Of the 106 patients, 18 were grade 0 (17.0%), 64 were grade 1 (60.4%), 17 were grade 2 (16.0%), and seven were grade 3 (6.6%). Therefore, 82 patients were assigned to the low-grade steatosis group and 24 patients were assigned to the high-grade steatosis group. Only one patient was suspected of iron overload on MRI examination; however, iron overload was not identified in the histopathological review.

#### Liver steatosis value in MR-PDFF, MRS, and pathology

The liver steatosis values were organized according to the measurement method used for the two patient groups (**Table 2**). There was a significant difference in liver steatosis values between the two groups (approximately 10.7–12.0% vs. 27.7–28.9%,  $P < 0.001$ ). Histopathologically, the mean value of the low-grade steatosis group was 17.3%, and that of the high-grade steatosis group was 55.2%, and there was a statistically significant difference (**Table 2**,  $P < 0.001$ ).

The agreement between the MR-PDFF and the MRS showed excellent reliability (ICC, 0.980–0.998;  $P < 0.001$ ) (**Table 3**). However, the agreement between MRI measurements

**Table 2.** Value of liver steatosis in MR-PDFF, MRS, and pathology in patients with suspected non-alcoholic fatty liver disease

Liver steatosis measurement	Low-grade steatosis (n = 82)		High-grade steatosis (n = 24)		P value
	Mean $\pm$ SD (%)	Range	Mean $\pm$ SD (%)	Range	
MRI					
PDFF, median	10.7 $\pm$ 6.7	1.6–25.8	27.7 $\pm$ 8.4	18.7–45.5	< 0.001
PDFF, mean	10.7 $\pm$ 6.7	0.8–25.8	27.4 $\pm$ 8.2	18.5–45.3	< 0.001
MRS, mean	12.0 $\pm$ 7.0	1.2–26.5	28.9 $\pm$ 8.1	20.0–46.6	< 0.001
Pathology	17.3 $\pm$ 13.3	0–60	55.2 $\pm$ 14.1	35–75	< 0.001

MR = magnetic resonance, MRI = magnetic resonance imaging, PDFF = proton density fat fraction, MRS = magnetic resonance spectroscopy, SD = standard deviation.

**Table 3.** The ICC between the liver steatosis measurement methods

Liver steatosis measurement methods	ICC	95% CI	P value
MR-PDFF median vs. MR-PDFF mean	0.998	0.997–0.999	< 0.001
MRS mean vs. MR-PDFF median	0.983	0.960–0.991	< 0.001
MRS mean vs. MR-PDFF mean	0.980	0.951–0.990	< 0.001
Pathology vs. MRS mean	0.740	0.315–0.875	< 0.001
Pathology vs. MR-PDFF median	0.726	0.179–0.877	< 0.001
Pathology vs. MR-PDFF mean	0.720	0.167–0.874	< 0.001

MR-PDFF = magnetic resonance-proton density fat fraction, MRS = magnetic resonance spectroscopy, ICC = intraclass correlation coefficient, CI = confidence interval.

and pathology showed moderate reliability (ICC, 0.720–0.740;  $P < 0.001$ ) (Table 3). The agreement between histologic steatosis grade and MR-PDFF steatosis grade according to Caussy et al.<sup>14</sup> showed very good agreement (weighted-kappa value = 0.873, 95% confidence interval, 0.800–0.946).

### Feature selection and diagnostic performance of liver steatosis classifiers using machine learning

Among the hundreds of variable radiomic features, important feature selection was performed using 20 repeated 10-fold stratified cross-validations and a random forest regressor. The important features extracted by each method and the diagnostic performance of the liver steatosis classifier are presented in Table 4 and Fig. 5.

#### Radiomics classifier

A total of 15 radiomic features were extracted (wavelet-LLL neighboring gray tone difference matrix (NGTDM) coarseness, original first-order mean, and original first-order 90 percentile), which were determined to be the three most important features. The AUROC and accuracy in discriminating between low-grade and high-grade steatosis using radiomics classifier were  $0.94 \pm 0.09$  and  $0.91 \pm 0.16$ , respectively.

#### Clinical feature classifier

Thirteen features were extracted, the three most important: ALT, albumin, and ferritin. The AUROC and accuracy of the clinical feature classifier were  $0.74 \pm 0.16$  and  $0.76 \pm 0.19$ , respectively.

#### Radiologic feature classifier

MRS values were extracted as more important features than the mean or median PDFF values. The AUROC and accuracy of the radiologic feature classifier alone were  $0.96 \pm 0.08$  and  $0.92 \pm 0.17$ , respectively.

**Table 4.** Diagnostic performances of liver steatosis classifiers and several important features of each classifier

The classifier of liver steatosis	AUROC	Accuracy	Feature	Feature importance
Radiomics	0.94 ± 0.09	0.91 ± 0.16	Wavelet-LLL NGTDM coarseness	0.09746 ± 0.01457
			Original first-order mean	0.09114 ± 0.01458
			Original first-order 90 percentile	0.09093 ± 0.01552
			Wavelet-LLH NGTDM busyness	0.08858 ± 0.02622
			Wavelet-LLL GLDM small dependence high gray level emphasis	0.07688 ± 0.01382
			Original NGTDM coarseness	0.06578 ± 0.01051
			Wavelet-LLL first-order mean	0.06385 ± 0.00955
			Original GLRLM short run high gray level emphasis	0.06104 ± 0.01941
			Original first-order median	0.05756 ± 0.01339
			Original NGTDM busyness	0.05702 ± 0.01813
			Wavelet-LLL first-order 90 percentile	0.05530 ± 0.01472
			Wavelet-LLH first-order 10 percentile	0.05473 ± 0.00616
			Original shape least axis length	0.05244 ± 0.01036
			Wavelet-HLL GLDM large dependence low gray level emphasis	0.04422 ± 0.01233
Wavelet-LLH GLDM large dependence low gray level emphasis	0.04306 ± 0.00574			
Clinical feature	0.74 ± 0.16	0.76 ± 0.19	Alanine aminotransferase	0.11550 ± 0.11550
			Albumin	0.10148 ± 0.10148
			Ferritin	0.09444 ± 0.09444
			Age	0.08985 ± 0.08985
			Total bilirubin	0.08641 ± 0.08641
			Triglycerides	0.08528 ± 0.08528
			Body mass index	0.08402 ± 0.08402
			Low-density lipoprotein	0.06506 ± 0.06506
			High-density lipoprotein	0.05990 ± 0.05990
			Platelet count	0.05657 ± 0.05657
			Aspartate aminotransferase	0.05628 ± 0.05628
			Alkaline phosphatase	0.05516 ± 0.05516
			Gamma-glutamyl transferase	0.05005 ± 0.05005
			Radiologic feature	0.96 ± 0.08
Mean of MR-PDFF	0.26170 ± 0.26170			
Median of MR-PDFF	0.19702 ± 0.19702			
Combination of all radiomic, clinical, and radiologic measures	0.96 ± 0.09	0.91 ± 0.22	Mean of MRS	0.27821 ± 0.27821
			Mean of MR-PDFF	0.18507 ± 0.18507
			Median of MR-PDFF	0.11865 ± 0.11865
			Wavelet-LLL first-order median	0.08026 ± 0.08026
			Original first-order mean	0.06910 ± 0.06910
			Wavelet-LLL first-order mean	0.05754 ± 0.05754
			Original GLDM small dependence high gray level emphasis	0.05693 ± 0.05693
			Wavelet-LLH NGTDM busyness	0.05607 ± 0.05607
Wavelet-LLL GLDM small dependence high gray level emphasis	0.05174 ± 0.05174			
Original NGTDM coarseness	0.04643 ± 0.04643			

Wavelet-xyz indicates a combination of high-pass (H) and low-pass (L) filters, such as wavelet-low high low (LHL) or wavelet-high high low (HHL).

AUROC = area under the receiver operating characteristic curve, NGTDM = neighboring gray tone difference matrix, GLDM = gray level dependence matrix, GLRLM = gray level run length matrix, MRS = magnetic resonance spectroscopy, MR-PDFF = magnetic resonance-proton density fat fraction.

#### *All combinations of radiomic, clinical, and radiologic classifiers*

Eight important features were extracted: MRS mean, MR-PDFF mean, and MR-PDFF median were extracted as the three most important features. The AUROC and accuracy of all combinations of variable features were  $0.96 \pm 0.09$  and  $0.91 \pm 0.22$ , respectively.

#### **Pairwise comparison of AUROCs of machine learning classifiers**

**Table 5** shows the pairwise comparison of the AUROC of the machine learning classifier using Delong's test. The virtually identical AUROCs of radiologic classifier and combination of all features classifiers were obtained (AUROC =  $0.96 \pm 0.09$  vs.  $0.96 \pm 0.08$ ,  $P = 0.279$ ). The AUROC of the radiomics classifier was  $0.94 \pm 0.09$ , and there was no statistically significant difference compared to the radiologic classifier ( $P = 0.400$ ) and the combination of all

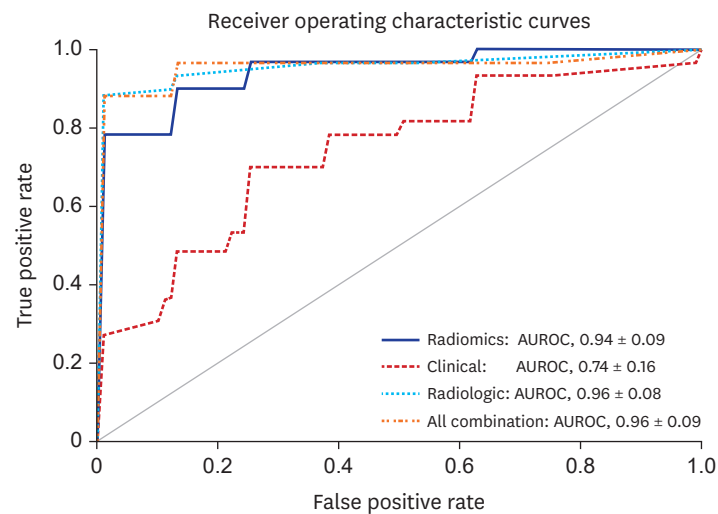


**Fig. 5.** Receiver operating characteristic curve for prediction of the grade of liver steatosis. AUROC = area under the receiver operating characteristic curve.

**Table 5.** Pairwise comparison of the AUROC of the machine learning classifier with Delong's test

Classifier models	AUROC	P value
Combination of radiomics, radiologic, and clinical features	0.96 ± 0.09	0.676
Radiomics	0.94 ± 0.09	
Combination of radiomics, radiologic, and clinical features	0.96 ± 0.09	0.279
Radiologic features	0.96 ± 0.08	
Combination of radiomics, radiologic, and clinical features	0.96 ± 0.09	< 0.001
Clinical features	0.74 ± 0.16	
Radiomics	0.94 ± 0.09	0.400
Radiologic features	0.96 ± 0.08	
Radiomics	0.94 ± 0.09	< 0.001
Clinical features	0.74 ± 0.16	
Radiologic features	0.96 ± 0.08	< 0.001
Clinical features	0.74 ± 0.16	

AUROC = area under the receiver operating characteristic curve.

feature classifiers ( $P = 0.676$ ). The clinical feature classifier exhibited the lowest diagnostic performance (AUROC =  $0.74 \pm 0.16$ ). There was a significant difference between the AUROC of the clinical feature classifier and those of the other classifiers ( $P < 0.001$ ).

## DISCUSSION

This study developed prediction models for liver steatosis in patients with suspected NAFLD based on radiomics, machine learning from MR fat quantification imaging, and various clinical features. This study showed that radiomics analysis of MR-PDFF (AUROC =  $0.94 \pm 0.09$ ) could accurately differentiate high-grade steatosis (grade 2 or grade 3) from low-grade steatosis (grade 0 or grade 1) in patients with suspected NAFLD and AUROC of MR-PDFF radiomics was comparable to that of radiologic measures ( $0.96 \pm 0.06$ ). Our study aimed to investigate the difference between MR-PDFF using ROI measurement, which is widely used as the gold standard, and radiomic analysis, which has recently been in the spotlight. However, the AUROC of the MR-PDFF radiomics analysis showed a slight decrease rather than an increase compared to conventional radiologic measures, without a statistical difference ( $P = 0.400$ ). Our results suggest that the current radiomics analysis under specific

conditions may have a lower AUROC than the existing simpler measurement method, despite the extra time and effort required. Dzyubak et al.<sup>35</sup> have already published a study using the auto-segmentation tool, which is the first step of radiomics analysis; however, if radiomics and machine learning software are embedded in picture archiving and communication systems, radiomics analysis can be applied more widely in the future.

In addition to hepatic tumors, several radiomics studies have been conducted on chronic liver disease, mainly focusing on the staging of liver fibrosis.<sup>17,36,37</sup> A radiomics analysis related to liver steatosis was only conducted in one study<sup>38</sup>; however, CT was used as an imaging modality. A limitation of the study by Naganawa et al.<sup>38</sup> was that it did not represent the whole liver using only a single slice and a single small ROI, which did not match the direction of the radiomic analysis, where whole-volume segmentation is important. Chronic liver disease is associated with changes in liver volume, morphology, and texture. Moreover, these changes can show spatial heterogeneity. Therefore, the authors' study could reflect the whole liver information and is the first radiomics study to predict the grade of steatosis using MR images, especially MR-PDFF images.

It is believed that it is very difficult to match the meaning of the radiomic feature values and terms that a radiologist interprets as MR-PDFF images one by one. In the fat fraction image of MR-PDFF, the liver appeared brighter as the degree of steatosis increased, correlated with the increase in signal intensity in the ROI measurement. In addition, as the degree of steatosis increases, vascular structures such as the hepatic vein and portal vein are observed with dark signal intensity; thus, the contrast with the liver parenchyma is clear. The most important feature was wavelet-LLL NGTDM coarseness,<sup>30</sup> which showed an average high value in low-grade steatosis, indicating a lower spatial change rate and a locally more uniform texture. Interestingly, the same second-order statistics, NGTDM Busyness,<sup>30</sup> showed a low value in low-grade steatosis, indicating no rapid changes in intensity between pixels and their neighborhood. These radiomics feature values were consistent with liver expression with homogeneous low signal intensity in low-grade steatosis MR-PDFF images. In contrast, the liver shows an overall bright signal intensity in high-grade steatosis. In such a bright background, if there are blood vessels observed as signal void or uneven steatosis areas observed as heterogeneous signal intensity, the liver is considered to represent a high NGTDM busyness feature and a low NGTDM coarseness feature. Additionally, features related to brightness, such as first-order mean and median, were naturally selected.

There are many studies on the correlation between MRS, MR-PDFF, and liver biopsy, which are representative methods for quantifying hepatic steatosis.<sup>14,39-42</sup> Although there were subtle differences in the results, both MRS and MR-PDFF showed an excellent correlation with the histologic grade of liver steatosis. Considering the liver volume included when measuring steatosis, it can be divided into MR-PDFF and radiomics, which can analyze the whole liver, and MRS and biopsy, which can analyze the limited volume.<sup>14</sup> Although liver biopsy with histological scoring is used as the gold standard for diagnosing hepatic steatosis, a biopsy could be insensitive to small but important changes in liver fat content due to sampling variability, broad grading categories, and inter- and intra-rater variability. These limitations can be equally applied to MRS. However, in our study, MRS had a higher ICC with pathologic steatosis than MR-PDFF, and MRS showed the highest feature importance among radiologic features. Several reasons can be hypothesized as to why MRS was selected as the test method that was best correlated with liver biopsy for grading liver steatosis. First, the right lobe, where MRS is measured mainly, is close to the liver biopsy site (segment 5/6). In contrast, MR-PDFF also included the left and right superior segments. Second, there may be statistical bias due

to the small number of subjects. Therefore, for the initial test of hepatic steatosis, it would be appropriate to perform MRS with MR-PDFF, which can evaluate the entire liver. For follow-up, it would be useful to observe changes in hepatic steatosis with non-invasive MR-PDFF.

Several demographic data showed significant differences between the low- and high-grade steatosis groups. ALT, albumin, and ferritin levels were the most important clinical features (Table 4). It can be confirmed that all these values were measured as statistically significant high values in the high-grade steatosis group (Table 1). Results, such as higher serum ALT, AST, ferritin, and obesity levels were confirmed to be in good agreement with the known laboratory and clinical risk factors related to the severity of NAFLD.<sup>43-45</sup> However, it cannot be used as a diagnostic tool to classify liver steatosis using only these clinical features (AUROC = 0.74 ± 0.16). These clinical features can be used as important markers in the setting of treatment monitoring after diagnosis or to increase the diagnostic conspicuity of patients suspected of NAFLD based on MR-PDFF. In our study, the high-grade steatosis group showed a younger age, and a higher albumin level was the opposite of known risk factors for NAFLD.<sup>45,46</sup> This may be due to the small number of patients in our study.

This study has several limitations that warrant further research. First, this study has the disadvantage of being a single-center study with a relatively small number of patients. As a result, the study population size was not sufficiently large to be divided into training and validation sets for use in the recent radiomic pipeline.<sup>47,48</sup> Second, no external validation for machine learning was performed, which limits the generalizability of our results. Third, selection bias may have been present due to the retrospective design of the study. Fourth, the grades of pathological steatosis in our study population were not equivalent, and there were more patients in grades 0–1 than in grades 2–3. Among them, 18 patients with less than 5% of hepatic steatosis confirmed through pathology were included in the low-grade steatosis group. Fifth, the inter- and intra-observer reliabilities of the multiple small- and whole-volume segmentation ROI measures could not be assessed. However, these shortcomings would have been overcome because multiple ROI drawings were performed up to nine times, and whole-volume segmentation was performed after sufficient training by a software applicator.

In conclusion, radiomic analysis using MR-PDFF provides a diagnostic performance comparable to that of conventional MR-PDFF analysis for the assessment of steatosis grading in patients with suspected NAFLD. Therefore, MR-PDFF-derived radiomics may provide a comparable alternative for grading liver steatosis in patients with suspected NAFLD.

## REFERENCES

1. Younossi ZM, Blissett D, Blissett R, Henry L, Stepanova M, Younossi Y, et al. The economic and clinical burden of nonalcoholic fatty liver disease in the United States and Europe. *Hepatology* 2016;64(5):1577-86. [PUBMED](#) | [CROSSREF](#)
2. Stål P. Liver fibrosis in non-alcoholic fatty liver disease - diagnostic challenge with prognostic significance. *World J Gastroenterol* 2015;21(39):11077-87. [PUBMED](#) | [CROSSREF](#)
3. Mitra S, De A, Chowdhury A. Epidemiology of non-alcoholic and alcoholic fatty liver diseases. *Transl Gastroenterol Hepatol* 2020;5(5):16. [PUBMED](#) | [CROSSREF](#)
4. Kang SH, Lee HW, Yoo JJ, Cho Y, Kim SU, Lee TH, et al. KASL clinical practice guidelines: management of nonalcoholic fatty liver disease. *Clin Mol Hepatol* 2021;27(3):363-401. [PUBMED](#) | [CROSSREF](#)

5. Lee YB, Ha Y, Chon YE, Kim MN, Lee JH, Park H, et al. Association between hepatic steatosis and the development of hepatocellular carcinoma in patients with chronic hepatitis B. *Clin Mol Hepatol* 2019;25(1):52-64.  
[PUBMED](#) | [CROSSREF](#)
6. Jang WY, Chung WJ, Jang BK, Hwang JS, Lee HJ, Hwang MJ, et al. Changes in characteristics of patients with liver cirrhosis visiting a tertiary hospital over 15 years: a retrospective multi-center study in Korea. *J Korean Med Sci* 2020;35(29):e233.  
[PUBMED](#) | [CROSSREF](#)
7. Bravo AA, Sheth SG, Chopra S. Liver biopsy. *N Engl J Med* 2001;344(7):495-500.  
[PUBMED](#) | [CROSSREF](#)
8. Kleiner DE, Brunt EM, Van Natta M, Behling C, Contos MJ, Cummings OW, et al. Design and validation of a histological scoring system for nonalcoholic fatty liver disease. *Hepatology* 2005;41(6):1313-21.  
[PUBMED](#) | [CROSSREF](#)
9. Bedossa P, Dargère D, Paradis V. Sampling variability of liver fibrosis in chronic hepatitis C. *Hepatology* 2003;38(6):1449-57.  
[PUBMED](#) | [CROSSREF](#)
10. Runge JH, Smits LP, Verheij J, Depla A, Kuiken SD, Baak BC, et al. MR Spectroscopy-derived proton density fat fraction is superior to controlled attenuation parameter for detecting and grading hepatic steatosis. *Radiology* 2018;286(2):547-56.  
[PUBMED](#) | [CROSSREF](#)
11. Imajo K, Kessoku T, Honda Y, Tomeno W, Ogawa Y, Mawatari H, et al. Magnetic resonance imaging more accurately classifies steatosis and fibrosis in patients with nonalcoholic fatty liver disease than Transient elastography. *Gastroenterology* 2016;150(3):626-637.e7.  
[PUBMED](#) | [CROSSREF](#)
12. Reeder SB, Cruite I, Hamilton G, Sirlin CB. Quantitative assessment of liver fat with magnetic resonance imaging and spectroscopy. *J Magn Reson Imaging* 2011;34(4):729-49.  
[PUBMED](#) | [CROSSREF](#)
13. Sellers R. MR LiverLab. [http://clinical-mri.com/wp-content/uploads/2016/11/How\\_I\\_do\\_it\\_LiverLab\\_Sellers\\_RSNA\\_MAGNETOM\\_Flash.pdf](http://clinical-mri.com/wp-content/uploads/2016/11/How_I_do_it_LiverLab_Sellers_RSNA_MAGNETOM_Flash.pdf). Updated 2016. Accessed April 5, 2022.
14. Caussy C, Reeder SB, Sirlin CB, Loomba R. Noninvasive, quantitative assessment of liver fat by MRI-PDFF as an endpoint in NASH trials. *Hepatology* 2018;68(2):763-72.  
[PUBMED](#) | [CROSSREF](#)
15. Gillies RJ, Kinahan PE, Hricak H. Radiomics: images are more than pictures, they are data. *Radiology* 2016;278(2):563-77.  
[PUBMED](#) | [CROSSREF](#)
16. Park HJ, Park B, Lee SS. Radiomics and deep learning: hepatic applications. *Korean J Radiol* 2020;21(4):387-401.  
[PUBMED](#) | [CROSSREF](#)
17. Sim KC, Kim MJ, Cho Y, Kim HJ, Park BJ, Sung DJ, et al. Diagnostic feasibility of magnetic resonance elastography radiomics analysis for the assessment of hepatic fibrosis in patients with nonalcoholic fatty liver disease. *J Comput Assist Tomogr* 2022;46(4):505-13.  
[PUBMED](#) | [CROSSREF](#)
18. Kim YK, Kwon OS, Her KH. The grade of nonalcoholic fatty liver disease is an independent risk factor for gallstone disease: an observational Study. *Medicine (Baltimore)* 2019;98(27):e16018.  
[PUBMED](#) | [CROSSREF](#)
19. Qayyum A, Nystrom M, Noworolski SM, Chu P, Mohanty A, Merriman R. MRI steatosis grading: development and initial validation of a color mapping system. *AJR Am J Roentgenol* 2012;198(3):582-8.  
[PUBMED](#) | [CROSSREF](#)
20. Chalasani N, Wilson L, Kleiner DE, Cummings OW, Brunt EM, Unalp A, et al. Relationship of steatosis grade and zonal location to histological features of steatohepatitis in adult patients with non-alcoholic fatty liver disease. *J Hepatol* 2008;48(5):829-34.  
[PUBMED](#) | [CROSSREF](#)
21. Yokoo T, Serai SD, Pirasteh A, Bashir MR, Hamilton G, Hernando D, et al. Linearity, bias, and precision of hepatic proton density fat fraction measurements by using MR imaging: a meta-analysis. *Radiology* 2018;286(2):486-98.  
[PUBMED](#) | [CROSSREF](#)
22. Zhao YZ, Gan YG, Zhou JL, Liu JQ, Cao WG, Cheng SM, et al. Accuracy of multi-echo Dixon sequence in quantification of hepatic steatosis in Chinese children and adolescents. *World J Gastroenterol* 2019;25(12):1513-23.  
[PUBMED](#) | [CROSSREF](#)

23. Jeon SK, Lee JM, Joo I, Park SJ. Quantitative ultrasound radiofrequency data analysis for the assessment of hepatic steatosis in nonalcoholic fatty liver disease using magnetic resonance imaging proton density fat fraction as the reference standard. *Korean J Radiol* 2021;22(7):1077-86.  
[PUBMED](#) | [CROSSREF](#)
24. Hamilton G, Yokoo T, Bydder M, Cruite I, Schroeder ME, Sirlin CB, et al. In vivo characterization of the liver fat <sup>1</sup>H MR spectrum. *NMR Biomed* 2011;24(7):784-90.  
[PUBMED](#) | [CROSSREF](#)
25. Ajmera V, Park CC, Caussy C, Singh S, Hernandez C, Bettencourt R, et al. Magnetic resonance imaging proton density fat fraction associates with progression of fibrosis in patients with nonalcoholic fatty liver disease. *Gastroenterology* 2018;155(2):307-310.e2.  
[PUBMED](#) | [CROSSREF](#)
26. Middleton MS, Heba ER, Hooker CA, Bashir MR, Fowler KJ, Sandrasegaran K, et al. Agreement between magnetic resonance imaging proton density fat fraction measurements and pathologist-assigned steatosis grades of liver biopsies from adults with nonalcoholic steatohepatitis. *Gastroenterology* 2017;153(3):753-61.  
[PUBMED](#) | [CROSSREF](#)
27. Middleton MS, Van Natta ML, Heba ER, Alazraki A, Trout AT, Masand P, et al. Diagnostic accuracy of magnetic resonance imaging hepatic proton density fat fraction in pediatric nonalcoholic fatty liver disease. *Hepatology* 2018;67(3):858-72.  
[PUBMED](#) | [CROSSREF](#)
28. Chen J, Talwalkar JA, Yin M, Glaser KJ, Sanderson SO, Ehman RL. Early detection of nonalcoholic steatohepatitis in patients with nonalcoholic fatty liver disease by using MR elastography. *Radiology* 2011;259(3):749-56.  
[PUBMED](#) | [CROSSREF](#)
29. Amadasun M, King R. Textural features corresponding to textural properties. *IEEE Trans Syst Man Cybern* 1989;19(5):1264-74.  
[CROSSREF](#)
30. van Griethuysen JJ, Fedorov A, Parmar C, Hosny A, Aucoin N, Narayan V, et al. Computational radiomics system to decode the radiographic phenotype. *Cancer Res* 2017;77(21):e104-7.  
[PUBMED](#) | [CROSSREF](#)
31. Çinarer G, Emiroğlu BG, Yurttakal AH. Prediction of glioma grades using deep learning with wavelet radiomic features. *Appl Sci* 2020;10(18):6296.  
[CROSSREF](#)
32. Kniep HC, Madesta F, Schneider T, Hanning U, Schönfeld MH, Schön G, et al. Radiomics of brain MRI: utility in prediction of metastatic tumor type. *Radiology* 2019;290(2):479-87.  
[PUBMED](#) | [CROSSREF](#)
33. Breiman L. Random forests. *Mach Learn* 2001;45(1):5-32.  
[CROSSREF](#)
34. Donner A, Zou G. Testing the equality of dependent intraclass correlation coefficients. *Statistician* 2002;51(3):367-79.  
[CROSSREF](#)
35. Dzyubak B, Li J, Chen J, Mara KC, Therneau TM, Venkatesh SK, et al. Automated analysis of multiparametric magnetic resonance imaging/magnetic resonance elastography exams for prediction of nonalcoholic steatohepatitis. *J Magn Reson Imaging* 2021;54(1):122-31.  
[PUBMED](#) | [CROSSREF](#)
36. Park HJ, Lee SS, Park B, Yun J, Sung YS, Shim WH, et al. Radiomics analysis of gadoteric acid-enhanced MRI for staging liver fibrosis. *Radiology* 2019;290(2):380-7.  
[PUBMED](#) | [CROSSREF](#)
37. Lan GY, Guo Y, Zhang XY, Cai XL, Shi Y. Value of radiomic analysis of data from magnetic resonance elastography for diagnosing fibrosis stages in patients with hepatitis B/C. *Chin J Acad Radiol* 2019;1(2):74-84.  
[CROSSREF](#)
38. Naganawa S, Enooku K, Tateishi R, Akai H, Yasaka K, Shibahara J, et al. Imaging prediction of nonalcoholic steatohepatitis using computed tomography texture analysis. *Eur Radiol* 2018;28(7):3050-8.  
[PUBMED](#) | [CROSSREF](#)
39. Achmad E, Yokoo T, Hamilton G, Heba ER, Hooker JC, Changchien C, et al. Feasibility of and agreement between MR imaging and spectroscopic estimation of hepatic proton density fat fraction in children with known or suspected nonalcoholic fatty liver disease. *Abdom Imaging* 2015;40(8):3084-90.  
[PUBMED](#) | [CROSSREF](#)

40. Idilman IS, Keskin O, Celik A, Savas B, Elhan AH, Idilman R, et al. A comparison of liver fat content as determined by magnetic resonance imaging-proton density fat fraction and MRS versus liver histology in non-alcoholic fatty liver disease. *Acta Radiol* 2016;57(3):271-8.  
[PUBMED](#) | [CROSSREF](#)
41. Di Martino M, Pacifico L, Bezzi M, Di Miscio R, Sacconi B, Chiesa C, et al. Comparison of magnetic resonance spectroscopy, proton density fat fraction and histological analysis in the quantification of liver steatosis in children and adolescents. *World J Gastroenterol* 2016;22(39):8812-9.  
[PUBMED](#) | [CROSSREF](#)
42. Idilman IS, Aniktar H, Idilman R, Kabacam G, Savas B, Elhan A, et al. Hepatic steatosis: quantification by proton density fat fraction with MR imaging versus liver biopsy. *Radiology* 2013;267(3):767-75.  
[PUBMED](#) | [CROSSREF](#)
43. Schindhelm RK, Diamant M, Dekker JM, Tushuizen ME, Teerlink T, Heine RJ. Alanine aminotransferase as a marker of non-alcoholic fatty liver disease in relation to type 2 diabetes mellitus and cardiovascular disease. *Diabetes Metab Res Rev* 2006;22(6):437-43.  
[PUBMED](#) | [CROSSREF](#)
44. Du SX, Lu LL, Geng N, Victor DW, Chen LZ, Wang C, et al. Association of serum ferritin with non-alcoholic fatty liver disease: a meta-analysis. *Lipids Health Dis* 2017;16(1):228.  
[PUBMED](#) | [CROSSREF](#)
45. Iqbal U, Perumpail BJ, Akhtar D, Kim D, Ahmed A. The epidemiology, risk profiling and diagnostic challenges of nonalcoholic fatty liver disease. *Medicines (Basel)* 2019;6(1):41.  
[PUBMED](#) | [CROSSREF](#)
46. Kawaguchi K, Sakai Y, Terashima T, Shimode T, Seki A, Orita N, et al. Decline in serum albumin concentration is a predictor of serious events in nonalcoholic fatty liver disease. *Medicine (Baltimore)* 2021;100(31):e26835.  
[PUBMED](#) | [CROSSREF](#)
47. Lambin P, Leijenaar RT, Deist TM, Peerlings J, de Jong EE, van Timmeren J, et al. Radiomics: the bridge between medical imaging and personalized medicine. *Nat Rev Clin Oncol* 2017;14(12):749-62.  
[PUBMED](#) | [CROSSREF](#)
48. Zwanenburg A, Vallières M, Abdalah MA, Aerts HJ, Andrearczyk V, Apte A, et al. The image biomarker standardization initiative: standardized quantitative radiomics for high-throughput image-based phenotyping. *Radiology* 2020;295(2):328-38.  
[PUBMED](#) | [CROSSREF](#)